PHYSICAL REVIEW B **83**, 100401(R) (2011)

# Thermopower and resistivity in ferromagnetic thin films near room temperature

A. D. Avery, Rubina Sultan, D. Bassett, D. Wei, and B. L. Zink*
*Department of Physics and Astronomy, University of Denver, Denver, Colorado 80208, USA*
(Received 4 January 2011; published 3 March 2011)

We present measurements of thermopower (Seebeck coefficient) and electrical resistivity of a wide selection of polycrystalline ferromagnetic films with thicknesses ranging from 60–167 nm. For comparison, a copper film of similar thickness was measured with the same techniques. Both the thermal and electrical measurements, made as a function of temperature from 77–325 K, are made using a micromachined thermal isolation platform consisting of a suspended, patterned silicon-nitride membrane. We observe a strong correlation between the resistivity of the films and the thermopower. Films with higher resistivity and residual resistivity ratios, indicating a higher concentration of static defects such as impurities or grain boundaries, with rare exception show thermopower of the same sign, but with absolute magnitude reduced from the thermopower of the corresponding bulk material. In addition, iron films exhibit the pronounced low-temperature peak in thermopower associated with magnon drag, with a magnitude similar to that seen in bulk iron alloys. These results provide important groundwork for ongoing studies of related thermoelectric effects in nanomagnetic systems, such as the spin Seebeck effect.

DOI: 10.1103/PhysRevB.83.100401 PACS number(s): 73.50.Lw, 72.10.Di, 73.43.Fj

## I. INTRODUCTION

Both the established field of spintronics and the emerging field of spin caloritronics[1] are exploring the next generation of logic and memory devices. Often designed with microscale and nanoscale magnetic samples, these devices are being developed both to improve energy efficiency and increase performance speed. This recent interest has generated increased focus on research into magnetic and thermal effects in a variety of sample types, including nanowires used for racetrack memory,[2] in multilayered films and nanowires,[3–5] and to manipulate spin degrees of freedom in thin films.[6–8] In order for these new technologies to advance, a thorough understanding of thermoelectric effects in candidate magnetic materials is necessary.

One important thermoelectric quantity being explored is the traditional Seebeck effect, or thermopower ($\alpha$), which is the voltage generated across a material when a difference in temperature is maintained at each end. When a temperature bias is applied across a sample, the electrons from the hot end of the sample diffuse into available energy states at the cooler end, setting up a potential difference. The theoretical equation describing $\alpha$ in the free-electron model is the Mott equation

$$\alpha(E) = \frac{\pi^2}{3}\frac{k_B^2 T}{e}\left[\frac{\partial \ln\sigma(E)}{\partial E}\right]_{E=E_F}, \quad (1)$$

where

$$\frac{\partial \ln\sigma(E)}{\partial E} = \frac{\partial A}{\partial E} + \frac{\partial \lambda}{\partial E}. \quad (2)$$

In the preceding equation, $\sigma$ is the electrical conductivity of a material, $T$ is the temperature, $A$ is the area of the Fermi sphere, and $\lambda$ is the electron mean-free path.[9] This equation relates changes in conductivity with changes in energy at the Fermi level and is sensitive to the changes in the number of available scattering centers and in the shape of the Fermi surface.

We have recently developed a micromachined thermal isolation platform that is a versatile and powerful tool for probing thermal properties and thermoelectric transport in a wide range of systems,[10] and is particularly well suited for studies of polycrystalline films ranging in thickness from ~10–200 nm. Although $\alpha$ in thin films can be measured by less involved means, this platform offers several advantages for thermopower measurements. Both the small size of the platform and the ability to make measurements of $\rho$ on the same sample removes uncertainties related to inhomogeneities between different samples. The small platform size also reduces radiation losses and offers better confidence that thermal gradients are controlled and measured with accuracy. Finally, the symmetry of the thermal platform greatly minimizes or eliminates any additional thermovoltage contribution from the leads that bridge the temperature gradient.

In the following sections, we first explain our measurement technique and layout of the thermal platform. We then present recent thermopower and electrical resistivity results for nickel, iron, permalloy (Ni-Fe), cobalt, and copper films with thicknesses ranging from 50–167 nm. Finally, we discuss these results and future directions for probing the fundamental physics governing thermoelectric transport in thin films and other nanostructures.

## II. EXPERIMENTAL DETAILS

Fabrication of the thermal isolation platform shown in Fig. 1 begins with a 500-nm-thick layer of amorphous silicon nitride (Si-N) deposited on both sides of a Si wafer by low-pressure chemical vapor deposition. A molybdenum layer is sputtered on the top of the wafer and then etched to form heaters, thermometers, and leads. Next, we etch the Si-N layer underneath the metal to form the platform features including two thermal islands, a Si-N bridge, and eight legs. The bridge serves as the thermal link between the two islands, and the legs connect the islands to the thermal bath, or frame. Finally, the entire platform is released by removing the bulk Si below the platform with an anisotropic Si etch. This leaves the Si-N structure suspended over a Si etch pit. Further fabrication details are published elsewhere.[10] Each island is patterned with a heater, a thermometer, and a lead for measuring thermopower and resistivity. The frame is also

 

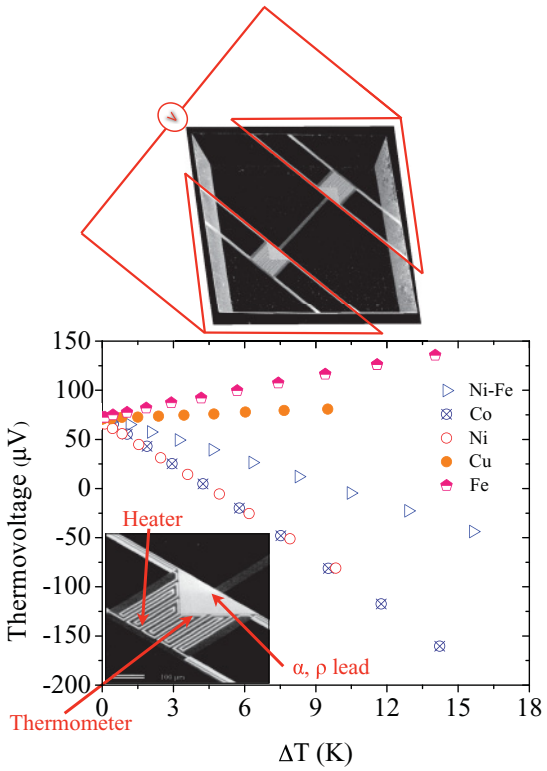


FIG. 1. (Color online) Top panel: Suspended thermal isolation platform with a schematic view of the circuit for measuring thermovoltage. Bottom panel: Thermovoltage ($\triangle V$) vs temperature change across the bridge ($\triangle T$) at 299 K for Fe, Cu, Co, Ni, and Ni-Fe films. Inset: Closeup of the island structure with heater and thermometer wires and the lead for measuring thermopower and resistivity.

patterned with a thermometer for measuring the reference temperature. At each reference point, a calibration reading is taken of all three integrated thermometers. All resistors, both heating and thermometry, have four wires running to them to allow four-wire measurements.

The first step in our technique is to establish a well-controlled thermal gradient across the platform. We create thermal gradients across the bridge using Joule heating provided by applying a series of currents to the heater on one island. After allowing sufficient time for thermal equilibrium, we measure the resistance of the thermometers on both islands and the frame. We convert from resistance ($R$) to temperature ($T$) for each of the thermometers by curve fitting the $T$ versus $R$ plot for each thermometer. $\triangle T$ is the temperature difference between the two islands. To measure absolute thermopower, we measured the thermoelectric voltage developed across the sample in response to the $\triangle T$. Thermopower is given by the slope of the $\triangle V$ versus $\triangle T$ plot at each reference temperature. For all measurements, we mount the platforms to a temperature-regulated oxygen-free high-purity copper block in a sample-in-vacuum cryostat. The block is surrounded by a copper radiation shield that provides an isothermal environment. The small area of the heated island dramatically reduces radiative heating that is usually problematic over 100 K.[10]

The magnetic films were deposited onto the thermal platform and additional separate Si-N substrates using electron-beam evaporation in an ultrahigh vacuum evaporation (UHV) chamber. The Cu film was thermally evaporated in the same UHV chamber and the 50-nm Ni film was rf sputtered at NIST, Boulder. Each film was deposited onto the bridge through a micromachined shadow mask that was aligned to allow the film to overlap the leads for measuring thermopower and electrical resistivity. The samples were grown at pressures between $10^{-7}$ and $10^{-8}$ torr. Resistivities of the substrates were measured using the Van der Pauw method and the film thicknesses were verified using profilometry.

Although the platform design removes lead resistance, it does not eliminate contact resistance. There are only two physical contacts for measuring film thermopower and resistivity on the platform. We have seen evidence of contact resistance after making measurements of the film on the bridge and comparing the film resistivity to the resistivity of a concurrently grown substrate. Successive measurements of resistivity over time have shown a time-dependent increase in resistance as well. However, subsequent measurements of film thermopower over time are repeatable. Therefore, we do not think this additional resistance is affecting the thermopower of the films.

## III. RESULTS AND DISCUSSION

Figure 2 compares literature values for bulk Ni to measured thermopower and resistivity results for the following films: 50-nm Ni, 83-nm Ni, two 75-nm Ni-Fe alloys, and a 60-nm Ni-Fe alloy. Data for several of these films were presented in an earlier study.[12] The data shown here for all samples are either from a repeated measurement or a result of reanalyzing the previous raw data with improved methods. Both the sputtered and evaporated Ni films display thermopower with the same sign as the bulk Ni (Ref. 11) and exhibit a temperature dependence similar to that of the bulk, but with smaller magnitude. Note that the roughly linear behavior with temperature (with negative slope) matches the expected behavior based on the Mott equation. Of the two Ni films measured, the film with greater disorder, as indicated by resistivity values, showed the smallest values for thermopower. In contrast, the thermopower measurements of Ni-Fe films display dramatically different temperature response when compared to a bulk Ni-Fe alloy

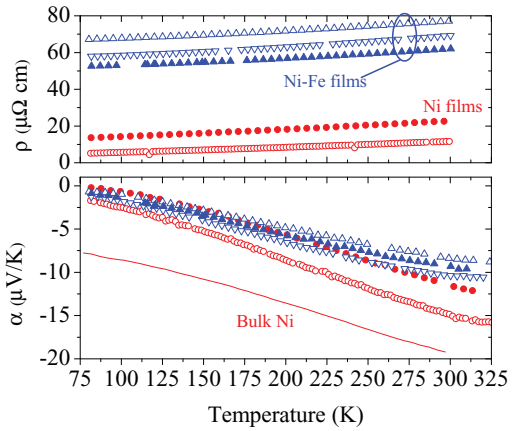


FIG. 2. (Color online) Measured $\rho$ and $\alpha$ of Ni (Filled circles: 83-nm evaporated film, Open circles: 50-nm sputtered film) and Ni-Fe alloy films (Open triangles: 75-nm films, Closed triangles: 60-nm film) compared to bulk literature values for Ni (Ref. 11) (solid lines).

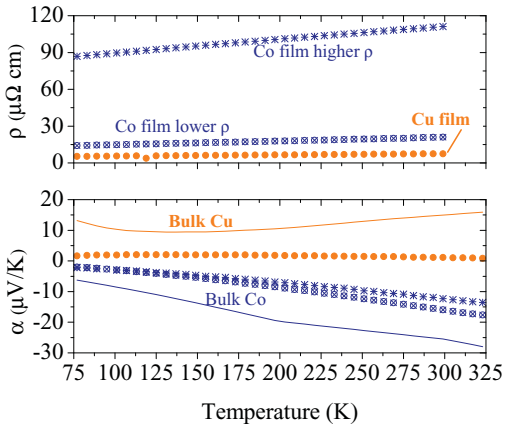


FIG. 3. (Color online) Measured $\rho$ and $\alpha$ of Co (Asterix: 167-nm thick film, x-filled circle: 75-nm thick film) and Cu films compared to bulk thermopower values for Co (Ref. 14) and Cu (Ref. 15).

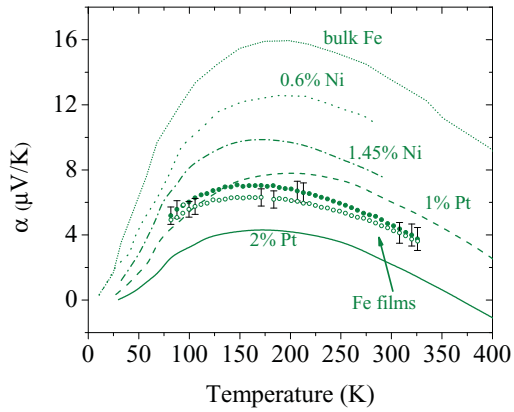


FIG. 4. (Color online) Fe $\alpha$ films (circles) compared to bulk data (lines 1–5) from Blatt *et al.* (Ref. 11) Line 1: bulk Fe; 2: 0.6% Ni; 3: 1.45% Ni; 4: 1% Pt; and 5: 2% Pt

reported by Ho[13] (these data are not shown in Fig. 2, but are negative with larger magnitude than bulk Ni and show signs of saturation near room temperature). The thermopower for the Ni-Fe films is negative as predicted, has a smaller magnitude, and a weaker temperature dependence than the bulk sample. One reason for this more complicated comparison between film and bulk may be the Ni-Fe composition of the films. The experimental permalloy films were not 80% Ni and 20% Fe as in the literature bulk sample, but evaporated from a ternary alloy with approximate composition 80% Ni, 15 % Fe, and 5% Mo. This difference in thermopower with respect to temperature could be due to additional scattering centers introduced by the Mo. The greater disorder in the alloys contributes additional electron scattering resulting in lower observed thermopower for these films. This smaller thermopower could also be due to changes in the shape of the Ni Fermi surface caused by the Fe and Mo. impurities

Thermopower and resistivity measurements for two Co films, 75 and 167 nm, and a 75-nm Cu film are presented in Fig. 3 with bulk literature thermopower values for Co (Ref. 14) and Cu.[15] The Co film grown at a base pressure of $6 \times 10^{-10}$ torr has a lower resistivity and larger thermopower than the second Co film grown at a base pressure of $1 \times 10^{-10}$. The Co film that was grown at a lower base pressure also has a temperature dependence closer to its bulk counterpart. Cu was chosen for its properties as a simple divalent nonmagnetic metal. Thermopower for Cu is predicted to be positive because its Fermi surface intersects the boundary of the first Brillouin zone. The measured thermopower for this Cu film is small and positive as expected. Both Cu and Co films, like the Ni, have smaller thermopower than bulk.

The 65- and 75-nm Fe films exhibit positive thermopower with a well-defined peak that we attribute to magnon drag. Similar to phonon drag, magnon drag appears when interactions between electrons and the magnon thermal current increase the voltage drop across a material at a given temperature. The two Fe films are plotted with several Fe and Fe alloys from Blatt *et al.*[11] in Fig. 4 illustrating this effect. In the paper by Blatt *et al.*, both magnetic and nonmagnetic metallic impurities diminished but did not destroy the magnon drag effect in bulk Fe. Similarly, our experiments show that magnons in Fe are far less sensitive than phonons to the disorder inherent in our films. Our results are a good indication that magnon drag still makes a clear contribution to thermopower even in disordered thin films. Magnons in the Fe films may also be responsible for the much smaller observed reduction in thermopower magnitude when compared to the other ferromagnetic films in this study. Although magnon drag seems to peak around 175 K in these films, magnons are still present throughout this temperature regime, resulting in larger film thermopower magnitudes in general.

These measurements clearly demonstrate coupling between resistivity and thermopower in magnetic films. Although it is tempting to explain the reduction in thermopower with changing resistivity using a constant offset or simple scaling factor, the observed differences in both thermopower magnitude and slope illustrate a more complicated relationship between the two quantities. Examination of Eqs. (1) and (2) suggests that $\alpha/T$ might scale simply with disorder, but this also appears not to be true for the data on this series of thin films. This prevents application of an effective electronic mean-free path model such as that recently used to explain reduction of thermopower in a nickel nanowire.[16] Additional measurements of a wider range of films over a wider range of temperature could shed light on what other effects play a role in the thermopower in thin metallic films.

## IV. CONCLUSION

We have presented a robust technique for making sensitive measurements of both thermopower and electrical resistivity on a thin-film sample. We have discussed experimental results for a simple metal film (Cu) as well as several ferromagnetic films with thicknesses ranging from 50–167 nm. All films measured displayed positive or negative thermopower in agreement with predicted theoretical values. With the exception of the Fe films, the magnitude of thermopower in the films was considerably reduced from values exhibited by similar bulk materials. The Fe films exhibited a smaller reduction in thermopower compared to bulk and a peak that were attributed to magnon effects in Fe. In this temperature range, disorder reduces the thermoelectric response to the heat flow caused by application of a thermal gradient across the film.

In the future, we plan to expand our measurements using a few simple modifications to the thermal isolation platform. Our technique can be easily applied to study other systems such as nanowires and multilayers, as well as other fundamental physical phenomena of interest such as spin currents. We will use this technique to probe the underlying physics governing transport in materials that are candidates for possible new spintronic or spin caloritronic components.

**ACKNOWLEDGMENTS**

The authors would like to thank Matthew R. Pufall at NIST, Boulder, for rf sputtering the 50-nm Ni sample; J. Rauch, A. Johnson, and G. Stiehl for assistance with data taking and equipment setup; and the National Science Foundation (Grant No. DMR-0847796) and the Nanoelectronics Research Initiative and Western Institute of Nanoelectronics for support.

*barry.zink@du.edu

[1]G. E. W. Bauer, A. H. MacDonald, and S. Maekawa, Solid State Commun. **150**, 459 (2010).

[2]S. Parkin, M. Hayashi, and L. Thomas, Science **320**, 190 (2008).

[3]M. Johnson and R. H. Silsbee, Phys. Rev. B **35**, 4959 (1987).

[4]M. Hatami, G. E. W. Bauer, Q. Zhang, and P. J. Kelly, Phys. Rev. B **79**, 174426 (2009).

[5]L. Gravier, A. Fábián, A. Rudolf, A. Cachin, J. E. Wegrowe, and J. P. Ansermet, J. Magn. Magn. Mater. **271**, 153 (2004).

[6]C. M. Jaworski, J. Yang, S. Mack, D. D. Awschalom, J. P. Heremans, and R. C. Myers, Nat. Mater. **9**, 898 (2010).

[7]J. Xiao, G. E. W. Bauer, K.-C. Uchida, E. Saitoh, and S. Maekawa, Phys. Rev. B **81**, 214418 (2010).

[8]K. Uchida, S. Takahashi, K. Harii, J. Ieda, W. Koshibae, K. Ando, S. Maekawa, and E. Saitoh, Nature (London) **455**, 778 (2008).

[9]J. M. Ziman, *Electrons and Phonons* (Oxford University, London, 1960).

[10]R. Sultan, A. D. Avery, G. Stiehl, and B. L. Zink, J. Appl. Phys. **105**, 043501 (2009).

[11]F. J. Blatt, D. J. Flood, V. Rowe, P. A. Schroeder, and J. E. Cox, Phys. Rev. Lett. **18**, 395 (1967).

[12]B. L. Zink, A. D. Avery, R. Sultan, D. Bassett, and M. R. Pufall, Solid State Commun. **150**, 514 (2010).

[13]C. Ho, T. Chi, R. Bogaard, T. Havill, and H. James, in *Thermal Conductivity 17*, Thermophysical Properties Division National Bureau of Standards, Vol. 17, edited by J. Hust (Plenum, New York, 1983), pp. 195–205.

[14]M. J. Laubitz and T. Matsumura, Can. J. Phys. **51**, 1247 (1973).

[15]D. MacDonald and W. Pearson, Proc. Phys. Soc., London **78**, 306 (1961).

[16]E. Shapira, A. Tsukernik, and Y. Selzer, Nanotechnology **18**, 485703 (2007).